JOURNAL OF COMPUTATIONAL PHYSICS 84, 247–254 (1989)

Note

Numerical Solution of Poisson's Equation for Rapidly Varying Driving Functions

I. Introduction

Fast Fourier transform algorithms (FFT) have made the use of the discrete Fourier transform (DFT) an attractive technique for the numerical solution of partial differential equations with a finite-difference representation [1]. In particular, this technique has been successfully applied to the solution of Poisson's equation in cartesian [2, 3] and cylindrical coordinates [4]. However, it is well known that the DFT gives rise to large errors in the solution of rapidly varying problems due to aliasing and Gibbs' oscillations [5]. Motivated by the need to develop a fast and accurate technique for solving Poisson's equation for rapidly varying conditions, we have developed a reconstruction algorithm for the FFT (RFFT) to minimize errors due to aliasing and Gibbs' oscillations. This is achieved by prescribing the behavior within the sampling intervals of the sampled functions. We have used the RFFT with the algorithm of Kunhardt and Williams [4] and obtained an algorithm for the solution of Poisson's equation in cylindrical coordinates and for rapidly varying conditions. This algorithm (reconstruction-Poisson) has been successfully applied to the solution of problems in which the space-charge density exhibits very steep gradients and large dynamic range [6].

The reconstruction Poisson algorithm for solving Poisson's equation in cylindrical coordinates is discussed in Section II. In Section III, the accuracy of the algorithm is illustrated by solving representative examples.

II. Description of Reconstruction—Poisson Algorithm

A. *Reconstruction Algorithm, RFFT*

Let $f(z)$ denote any real function such that $f(z)=0$, for $z \geqslant a$ and $z \leqslant 0$, with Fourier transforms, $F(\kappa)$, given by

$$F(\kappa)=\int_0^a f(z)\, e^{i\kappa z}\, dz. \tag{1}$$

0021-9991/89 $3.00
Copyright © 1989 by Academic Press, Inc.
All rights of reproduction in any form reserved.

Suppose that $f(z)$ is digitized by choosing $N+1$ equally spaced samples, with grid size Δz, given by

$$\Delta z = a/N. \tag{2}$$

The maximum frequency, κ_m, that can be represented by this sampling period is

$$\kappa_m = \pi/\Delta z.$$

Let

$$\Gamma_s(\kappa) = \begin{cases} 1, & |\kappa| \leqslant \kappa_m \\ 0, & \text{otherwise} \end{cases} \tag{3}$$

be the Fourier transform of $\gamma_s(z)$, where

$$\gamma_s(z) = \frac{1}{2\pi} \int_{-\kappa_m}^{\kappa_m} e^{-i\kappa z}\, d\kappa. \tag{4}$$

If there is no aliasing error for the sampled signals, then $\Gamma_s(\kappa) F(\kappa)$ is the digitized Fourier transform for $|\kappa| \leqslant \kappa_m$. The function corresponding to $\Gamma_s(\kappa) F(\kappa)$ in the space domain is

$$f_s(z) = \int_0^a f(z')\, \gamma_s(z - z')\, dz', \tag{5}$$

where $f_s(z)$ is a κ_m-band-limited function of $f(z)$.

Let $f_d(z)$ be the digitized form of $f(z)$ which has a constant value, f_r, in an interval, where $0 \leqslant r \leqslant N$. The cell boundaries of cell r is $(r - 1/2)\,\Delta r$ and $(r + 1/2)\,\Delta r$. Assuming that the sampling error is less then ε, then

$$|f(z) - f_d(z)| < \varepsilon, \qquad 0 \leqslant z \leqslant a. \tag{6}$$

To approximate $f_s(z)$, we use a function, $\int_0^a f_d(z')\, \gamma_s(z - z')\, dz'$, which yields the best result for this given sampling period. From Schwarz' inequality and Eqs. (4)–(6), we find the error to be

$$\left| f_s(z) - \int_0^a f_d(z')\, \gamma_s(z - z')\, dz' \right| \leqslant \varepsilon \cdot \frac{\kappa_m}{\pi} \cdot a = \varepsilon N, \qquad 0 \leqslant z \leqslant a. \tag{7}$$

For sufficiently small ε, this results in a good approximation. Then,

$$\begin{aligned} f_s(z) &\approx \int_0^a f_d(z')\, \gamma_s(z - z')\, dz' \\ &= \sum_{r=0}^{N} f_r \int_{\text{cell } r} \gamma_s(z - z')\, dz' \\ &= \frac{1}{2\pi} \int_{-\kappa_m}^{\kappa_m} \left[\left(\Delta z \sum_{r=1}^{N-1} f_r e^{ir\kappa\, \Delta z} \right) \operatorname{sinc}\left(\frac{\kappa\, \Delta z}{2} \right) \right] e^{-i\kappa z}\, d\kappa, \end{aligned} \tag{8}$$

where

$$\operatorname{sinc}\left(\frac{\kappa\,\Delta z}{2}\right)=\sin\left(\frac{\kappa\,\Delta z}{2}\right)\Big/\left(\frac{\kappa\,\Delta z}{2}\right).$$

Thus, from Eq. (8) we find that the RFFT of a function is obtained by taking the FFT of the digitized function and multiplying it with a sinc function. This procedure minimizes aliasing errors.

To reduce the errors due to Gibbs' oscillation, we approximate $f_s(z)$ by a constant on each of the $N-1$ cells. This constant is obtained by averaging the signal in a cell. This average, f_j^a, is defined as

$$f_j^a=\frac{1}{\Delta z}\int_{(j-1/2)\,\Delta z}^{(j+1/2)\,\Delta z} f_s(z)\,dz, \qquad 1\leqslant j\leqslant N-1.$$

Using Eq. (8), we find

$$\begin{aligned} f_j^a &= \frac{1}{2\pi\,\Delta z}\int_{-\kappa_m}^{\kappa_m}\left[\left(\Delta z\sum_{r=1}^{N-1} f_r e^{i\kappa r\,\Delta z}\right)\operatorname{sinc}\left(\frac{\kappa\,\Delta z}{2}\right)\right]\int_{(j-1/2)\,\Delta z}^{(j+1/2)\,\Delta z} e^{-i\kappa z}\,dz\,d\kappa \\ &= \frac{1}{2\pi}\int_{-\kappa_m}^{\kappa_m} e^{-i\kappa j\,\Delta z}\left[\sum_{r=1}^{N-1}\Delta z f_r e^{i\kappa r\,\Delta z}\operatorname{sinc}\left(\frac{\kappa\,\Delta z}{2}\right)\right] \\ &\quad\times\operatorname{sinc}\left(\frac{\kappa\,\Delta z}{2}\right)d\kappa, \qquad 1\leqslant j\leqslant N-1. \end{aligned} \tag{9}$$

Note that f_j^a is represented by a constant value in an analog fashion. Thus, implementation of the inverse RFFT is achieved by multiplying the signal in the frequency domain with a sinc function as shown in Eq. (9).

The above derivation is summarized as follows:

1. In the transformation from physical to Fourier space, we have used a stepwise function (constant on each cell) to approximate the charge function in space. For the functions which are not stepwise, we have derived a maximum error caused by this approximation from Eqs. (3) to (7). Equation (7) can be used as a guide for the user to choose the sampling period to satisfy the accuracy he needs. The bandlimited function and Schwarz's inequality have been used to drive the upper error limit.

2. In the transformation back from Fourier space to a sampled function in physical space, we have no knowledge about the form of the resulting function. In order to reduce the unrealistic Gibbs' oscillations, we average the analytic resulting function on each interval, then get a stepwise analytic resulting function. As will be seen in the test cases, this approach results in a better approximation to the analytic solution, although the form of the analytic solution is not a stepwise function.

B. *Poisson Algorithm*

The potential, ϕ, in cylindrical coordinates satisfies Poisson's equation,

$$\frac{1}{r}\partial_r(r\partial_r\phi(r, z)) + \partial_z^2\phi(r, z) = -\rho(r, z)/\varepsilon_0 \tag{10}$$

subject to the boundary conditions $\phi(r, 0) = \phi(r, a) = 0$, where $0 \leqslant z \leqslant a$ and $0 \leqslant r \leqslant \infty$. In the algorithm of Kunhardt and Williams [4] (subsequently referred to as the KW algorithm), Eq. (10) is solved by expanding the functions ϕ and ρ as follows:

$$\phi(r, z) = \sum_{n=0}^{N-1} \phi_n^*(r) \sin\frac{n\pi}{a} z \tag{11}$$

$$\rho(r, z) = \sum_{n=0}^{N-1} \rho_n^*(r) \sin\frac{n\pi}{a} z. \tag{12}$$

Substituting Eqs. (11) and (12) into a z-discretized form of (10), and using the orthogonality properties of the sin functions, we obtain for ϕ_n^*,

$$\partial_r^2\phi_n^* + \frac{1}{r}\partial_r\phi_n^* + \frac{2}{\Delta z^2}\left(\cos\frac{n\pi}{N} - 1\right)\phi_n^* = -\frac{\rho_n^*(r)}{\varepsilon_0}. \tag{13}$$

In the reconstruction Poisson algorithm (subsequently referred to as the RP algorithm), we proceed to solve Eq. (13) as follows. From Eqs. (8) and (12), we find

$$\rho_n^*(r) = \rho_n(r)\,\mathrm{sinc}\left(\frac{n\pi}{a}\frac{\Delta z}{2}\right), \tag{14}$$

where $\rho_n(r)$ is obtained from $\rho(r, z)$ by using an FFT algorithm. Equation (13) is then solved by using a set of cubic polynomial spline functions that are chosen to satisfy the equation and continuity conditions (through the second derivative) at each grid point [4]. Once ϕ_n^* is obtained, $\phi(r, z)$ is found by taking the inverse FFT of $\phi_n(r)$ given by

$$\phi_n(r) = \phi_n^*\,\mathrm{sinc}\left(\frac{n\pi}{a}\frac{\Delta z}{2}\right). \tag{15}$$

FIG. 1. Numerical axial field, E_z, arising from a charge uniformly distributed in a disk with dimensions $0.085\text{ cm} \leqslant z \leqslant 0.105\text{ cm}$, $0 \leqslant r \leqslant 0.055\text{ cm}$. (a) Input charge density for $0 \leqslant r \leqslant 0.055$ cm. (b) Analytic solution for E_z on axis. (c) Errors incurred in the solution of Eq. (10) using the RP algorithm (solid line) and the KW algorithm (+). Only 40 gridpoints are plotted to show the difference clearly.

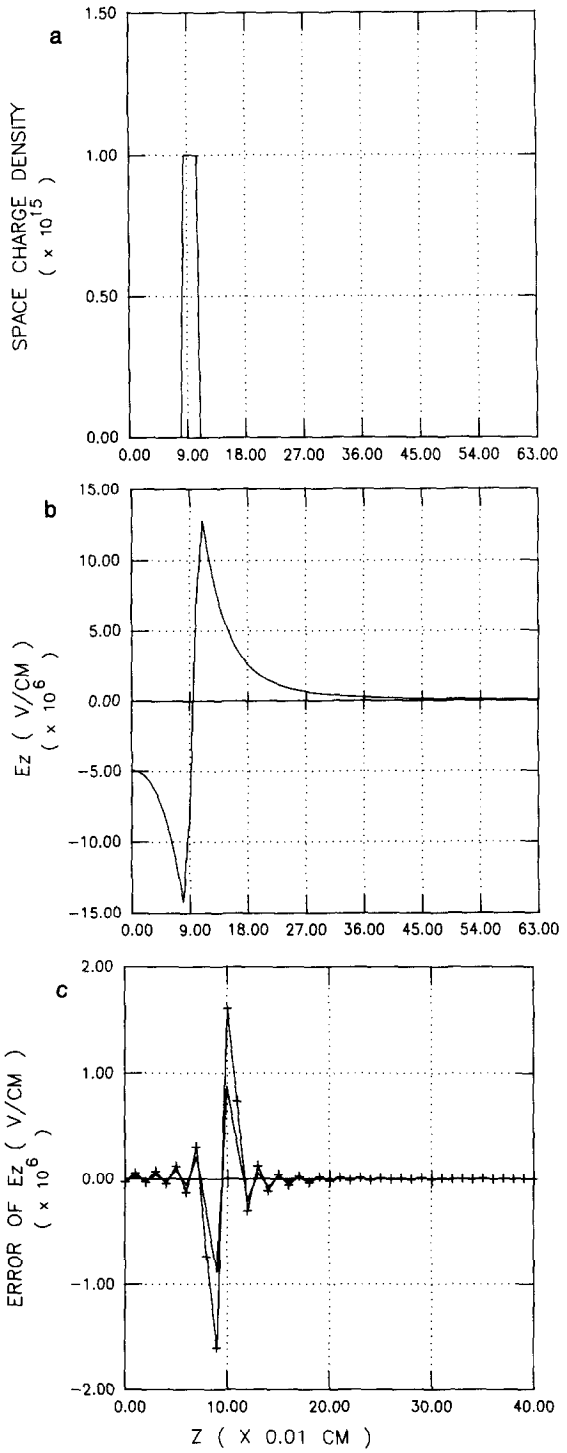
a
SPACE CHARGE DENSITY (x 10^15)
1.50
1.00
0.50
0.00
0.00 9.00 18.00 27.00 36.00 45.00 54.00 63.00
b
Ez (V/CM) (x 10^6)
15.00
10.00
5.00
0.00
-5.00
-10.00
-15.00
0.00 9.00 18.00 27.00 36.00 45.00 54.00 63.00
c
ERROR OF Ez (V/CM) (x 10^6)
2.00
1.00
0.00
-1.00
-2.00
0.00 10.00 20.00 30.00 40.00
Z (X 0.01 CM)

III. Test Results

The algorithm discussed in Section II has been tested on a spatial grid containing 65 points uniformly spaced along the z-direction, and 84 points along the r-direction. In the z-direction, two electrodes locate at $z=0$ and 0.64 cm, with $\Delta z=0.01$ cm. The ϕ and ρ are zero at electrodes. In the r-direction, grid points 1 through 64 are uniformly spaced, with $\Delta r=0.01$ cm; whereas grid points >64 are spaced with exponentially increasing Δr. To illustrate the algorithm, two test cases have been chosen. These cases exemplify situations which result in large errors from aliasing and Gibbs' oscillation. The first case is a disk with dimensions $0\leqslant r\leqslant 0.055$ cm, $0.085\text{ cm}\leqslant z\leqslant 0.105$ cm. The charge is uniformly distributed inside the disk and has a density of 10^{15} cm^{-3}. To show the accuracy of the RP algorithm, the axial field on axis, E_z ($E_z=-\partial\phi/\partial z$), has been calculated and compared to that obtained by two other methods, namely, analytic and the KW algorithm [4]. The analytic solution is obtained by summing the E_z of the disk and its images and shown in Fig. 1(b) [7]. The errors incurred with the KW and RP algorithms are shown in Fig. 1(c). As can be seen, the RP algorithm results in a significant reduction in the error for the potential at the steep edges of the charge distribution.

The second case considered represents a more stringent test. In this case, the charge is uniformly distributed in a disk of dimension Δz, Δr ($0.085\text{ cm}\leqslant z\leqslant 0.095$ cm and $0\leqslant r\leqslant 0.055$ cm). The charge density for the results shown in Fig. 2(a) is 10^{15} cm^{-3}. The analytic solution for this case is shown in Fig. 2(b). We expect the numerical solutions to show more overshoots and undershoots than for test case 1. From the error plots in Fig. 2(c), the RP algorithm is shown to yield superior results to those obtained from the direct method, especially near the charge distribution. At the grid point where maximum undershoot occurs, the error has been reduced from 22% (KW algorithm) to 12% (RP algorithm).

Finally, the differences in the CPU time between the KW and RP algorithm is negligible.

Acknowledgments

C. Wu thanks D. Youla for a number of stimulating discussions. This work has been supported by the U.S. Office of Naval Research (ONR).

Fig. 2. Numerical results for the axial electric field, E_z, arising from a charge uniformly distributed in a disk with dimensions $0.085\text{ cm}\leqslant z\leqslant 0.095$ cm, $0\leqslant r\leqslant 0.055$ cm. (a) Input charge density for $0\leqslant r\leqslant 0.055$ cm. (b) Analytic solution for E_z on axis. (c) Errors incurred in the numerical solution of Eq. (10) using the RP algorithm (solid line) and the KW algorithm (+). Only 40 gridpoints are plotted to show the difference clearly.

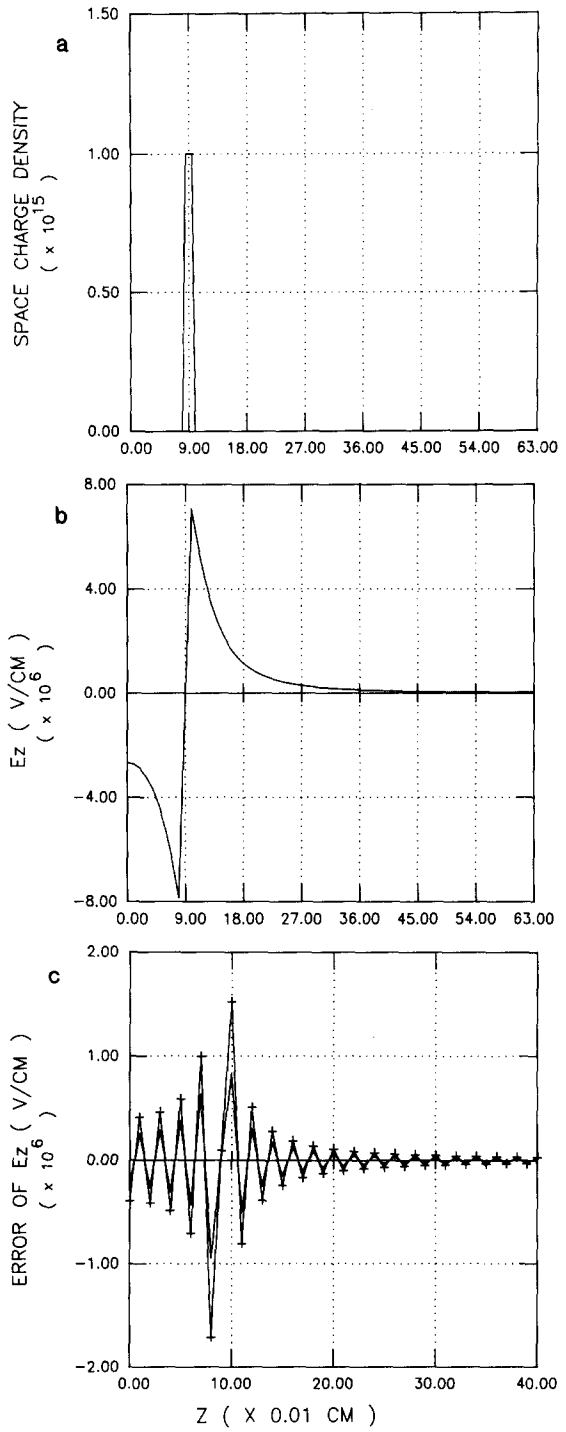
a
SPACE CHARGE DENSITY
(x 10^15)
1.50
1.00
0.50
0.00
0.00 9.00 18.00 27.00 36.00 45.00 54.00 63.00
b
Ez (V/CM)
(x 10^6)
8.00
4.00
0.00
-4.00
-8.00
0.00 9.00 18.00 27.00 36.00 45.00 54.00 63.00
c
ERROR OF Ez (V/CM)
(x 10^6)
2.00
1.00
0.00
-1.00
-2.00
0.00 10.00 20.00 30.00 40.00
Z (X 0.01 CM)

REFERENCES

1. L. COLLATZ, *The Numerical Treatment of Differential Equations*, (Springer-Verlag, New York 1966), p. 542.
2. R. W. HOCKNEY, *J. Assoc. Comput. Mach.* **12**, 95 (1965).
3. R. C. LE BAIL, *J. Comput. Phys.* **9**, 440 (1972).
4. E. E. KUNHARDT AND P. F. WILLIAMS, *J. Comput. Phys.* **57**, 403 (1985).
5. A. PAPOULIS, *Circuits and Systems: A Modern Approach* (Holt, Rinehart & Winston, New York, 1980), p. 376.
6. C. WU AND E. E. KUNHARDT, *Phys. Rev. A* **37**, 4396 (1988).
7. J. D. JACKSON, *Classical Electrodynamics* (Wiley, New York, 1975), p. 54.

RECEIVED April 28, 1988; REVISED October 3, 1988

C. WU

Electrical Engineering Department
Auburn University
Alabama 36849

E. E. KUNHARDT

Weber Research Institute
Polytechnic University
Route 110, Farmingdale
New York 11735